




# Amoxicillin Loaded Hollow Microparticles in the Treatment of Osteomyelitis Disease Using Single-Nozzle Electrospinning

Esra Altun<sup>1,2</sup> · Mehmet Onur Aydogdu<sup>1,2</sup> · Fatma Koc<sup>3</sup> · Ozlem Kutlu<sup>4</sup> · Devrim Gozuacik<sup>5</sup> · Sevil Yucel<sup>6</sup> · Oguzhan Gunduz<sup>2,7</sup> 

Published online: 2 July 2018

© Springer Science+Business Media, LLC, part of Springer Nature 2018

## Abstract

In this study, hollow microparticles were produced with polymethylsilsesquioxane/chitosan/bovine hydroxyapatite/hexagonal boron nitride (PCBB) polyblend using single-nozzle electrospinning method. Also, hollow microparticles are loaded with amoxicillin (AMX) and their drug delivery capabilities have been studied according to a treatment of osteomyelitis disease. The morphology, chemical groups, particle size, antimicrobial activity, and AMX drug release were systematically studied using scanning electron microscopy (SEM), optical microscopy, Fourier transformation infrared spectroscopy (FTIR), hollow microparticle size measurements, antimicrobial activity test, and UV spectroscopy. In vitro biocompatibility was analyzed with human bone osteosarcoma (U2OS) cell line. This present work can help in the design of a drug delivery platform for antimicrobial effect and bone repair at the same time for osteomyelitis disease treatment.

**Keywords** Single-nozzle electrospinning · Hollow microparticles · Osteomyelitis · Drug delivery · Bone tissue engineering

## 1 Introduction

Hollow microparticles have gained great interests for micro-encapsulation and have been used in both drug delivery and biomedical applications for decades [1]. They have become

popular because of their characteristic features, for instance, having a high surface to volume ratio and low density [2]. The size of pores in the hollow side of microparticles showing a huge difference in the encapsulation and delivery of functional materials [3] and the hollow particles with large passage holes above 10 nm are highly desired for applications containing biomacromolecules [4]. Many of the current techniques were used to produce microparticles, such as organic templates, inorganic templates, soft templates, and spray methods [5–10] aiming the different therapeutic solutions like drug delivery, bioencapsulation, catalyst, photonics, and additionally, in food and beverages [11–14]. One of the production methods of producing the hollow microparticles is electrohydrodynamic spraying method. The method uses electrical force to spraying towards gravity to into glass vials containing simulated body fluid (SBF) and ethanol [3] or onto a microscope slide containing distilled water [4]. Despite that, electrohydrodynamic spinning or electrospinning is a method that using electrical force to spraying towards or against gravity onto a collector. Electrospinning method has been widely used to produce ultrafine fibers with diameters ranging from tens of nanometers to several microns [15]. Its characteristic features made the electrospinning one of the most prominent modern methods of fiber and scaffold production for drug delivery [16] studies. In this study, single-nozzle electrospinning method (against gravity) is presented as a

✉ Oguzhan Gunduz  
oguzhan@marmara.edu.tr

<sup>1</sup> Department of Metallurgical and Materials Engineering, Institute of Pure and Applied Sciences, Marmara University, Goztepe Campus, 34722 Istanbul, Turkey

<sup>2</sup> Advanced Nanomaterials Research Laboratory, Department of Metallurgical and Materials Engineering, Marmara University, Goztepe Campus, 34722 Istanbul, Turkey

<sup>3</sup> Department of Medical Microbiology, Medipol University, Beykoz, 34810 Istanbul, Turkey

<sup>4</sup> Nanotechnology Research and Application Center, EFSUN-Center of Excellence for Functional Surfaces and Interfaces for Nano Diagnostic, Sabanci University, Tuzla, 34956 Istanbul, Turkey

<sup>5</sup> Molecular Biology Genetics and Bioengineering Program, Sabanci University, Tuzla, 34956 Istanbul, Turkey

<sup>6</sup> Department of Bioengineering, Yildiz Technical University, Esenler, 34220 Istanbul, Turkey

<sup>7</sup> Department of Metallurgical and Materials Engineering, Marmara University, Goztepe Campus, 34722 Istanbul, Turkey

method for production of drug-loaded hollow microparticles without fibers.

With the purpose of delivering, polymeric carriers can transport drugs to the site of action and, when drugs interact with other molecules, these molecules could cause a change in the chemical structure of the active ingredient, while causing it to lose its pharmaceutical action [17]. When it comes to design a new drug delivery system, various polymers are widely used for drug delivery research due to their effectiveness of delivering the drug and increase the therapeutic benefit, while minimizing side effects. Various biodegradable and non-biodegradable polymers have been used for drug delivery systems, such as polyesters, polyorthoesters, polyanhydrides, and polycarbonates [18]. Among these polymers, polymethylsilsesquioxane (PMSQ) is a promising polymer due to its good biocompatibility, non-toxicity, and chemical stability and hydrophobicity [19–24] and used in this study.

Chitosan (Ch) is a natural polysaccharide obtained from chitin with deacetylation and often used in combination with other polymers [25] for drug delivery systems [26]. Owing to it is polycationic and non-toxic mucoadhesive polymer features, it helps to deliver the drug and safe to use [27–29]. However, its bioactivity needs to be improved for tissue studies and should be combined with other bioactive materials. Hydroxyapatite (HA) is a good choice for combining with Ch due to its being a main inorganic component of natural bone with its strong characteristics such as biocompatibility, osteoconductivity, and bioactivity [30]. It has the ability to provide direct bonding to the bone tissue, and it is one of the most efficient biomaterials to use as a drug carrier [31, 32] as well as bone substitute [33, 34]. However, using the bovine-derived hydroxyapatite (BHA), instead of the HA, will result

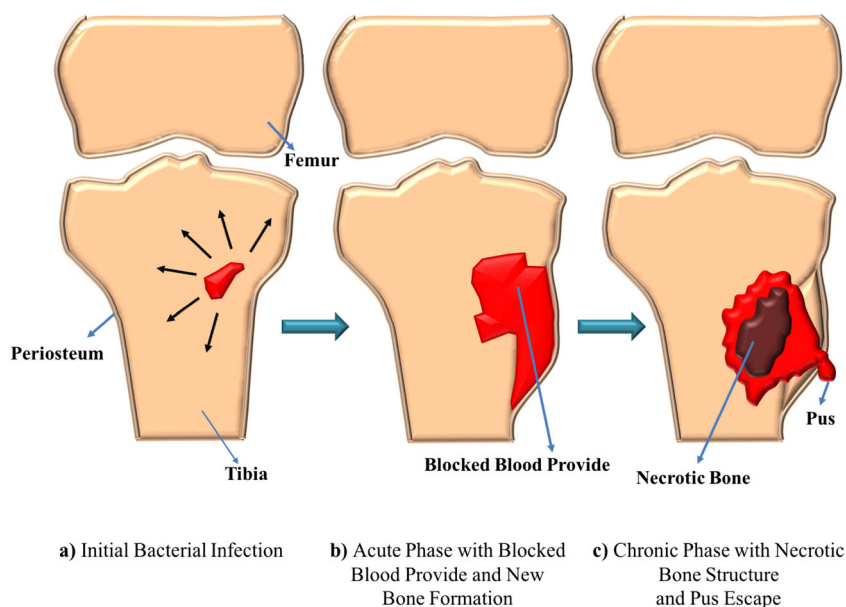
in stronger mechanical and structural properties [35], and in the present study, it has been used for these features.

Hexagonal boron nitride (hBN) has extensive application areas because of its beneficial properties, for instance, high chemical resistance, high thermal resistance, lubricity, and slipperiness [36]. In the present work, hBN's drug delivery potential with combining PMSQ, Ch, and BHA have been studied.

Bone infection or osteomyelitis (Fig. 1) is a bacterial infection of the bone [37]. Adults or children can be infected by osteomyelitis, after trauma, surgery, or insertion of a joint prosthesis, diabetic foot infections, and hematogenous origin among pathogenic microorganisms [38]. Recovery rates of antimicrobial therapy in most infectious diseases, including chronic osteomyelitis, have not yet been achieved in bone and joint infections owing to the physiological and anatomical characteristics of bone [39]. *Staphylococcus aureus* is by far the most commonly involved virulent bacteria for osteomyelitis cases, and there are many studies to understand the mechanisms of *S. aureus* in the pathogenesis of osteomyelitis [40–42]. Staphylococcal osteomyelitis accounts for rarely 2.5 out of every 1000 hospital admissions, with annual occurrence estimates ranging from 1 in 5000 to 1 in 10,000 in children [43, 44].

Acute osteomyelitis (clinically to a newly recognized bone infection) cases can be treated with antibiotics alone [45]. However, successful treatment of chronic osteomyelitis (clinically to a relapsed or long-standing bone infection) requires optimal surgical removing the diseased tissue and properly targeting of the tissue with antimicrobial regimens; otherwise, *S. aureus* can re-emerge itself due to its resistance to pretty much every available antibiotic is rapidly becoming a reality [46]. Amoxicillin (AMX) was preferred in the present work as

**Fig. 1** Schematic illustration for osteomyelitis disease at the knee. **a** Initial bacterial infection to the tibia. **b** Acute phase with blocked blood supply and new bone formation at the knee. **c** Chronic phase with necrotic bone structure and pus escape from the knee



a model drug because it could increase the period of active drug absorption in the extracellular fluid, so extending the dosing interval while ensuring antimicrobial activity and has essential remedy results on bone infection treatments [47–49]. Successful treatment of infections with AMX drug after osteomyelitis due to diabetic foot infections [50] and staphylococcal osteomyelitis in a rat model [51] also has been reported.

In this study, novel hollow microparticles with  $50 \pm 10$ - $\mu\text{m}$ -size diameter were produced with fiber to hollow microparticle transition using the single-nozzle electrospinning method for model drug (AMX) encapsulation, storage, and release to bone tissue for treatment of osteomyelitis disease.

## 2 Materials and Methods

### 2.1 Materials

PMSQ was purchased from WACKER, Germany. Chitosan (Ch), acetic acid, and dichloromethane (DCM) were all obtained from Sigma-Aldrich (St. Louis, MO, USA) and used without further purification. Bovine hydroxyapatite (BHA) was provided from Advanced Nanobiomaterials Research Laboratory, Marmara University (Istanbul, Turkey). hBN was supplied by American Elements Company, Los Angeles, CA, USA ( $A_p < 1 \mu\text{m}$ ). Amoxicillin (AMX; MW 365.4 g/mol) and phosphate-buffered saline (PBS) were also obtained from Sigma-Aldrich (Germany). Milli-Q was used during the experiments. Hoechst 33342 (H3570) and MitoTracker Red (M7512) were purchased from Thermo Fisher Scientific (USA). Dulbecco's modified Eagle's medium (DMEM) was from Sigma-Aldrich (D5671-Germany). L-glutamine (BIO3–020-1B), penicillin/streptomycin (BIO3–031-1B), and trypsin-EDTA (BIO3–050-1A) were purchased from Biological Industries (Israel). Fetal bovine serum (FBS) was purchased from BioWest (S1810-USA). Phosphate-buffered saline (PBS-17-516F, pH = 7.4) without calcium or magnesium was purchased from Lonza (USA). Human bone osteosarcoma cell line (U2OS-HTB-96) was purchased from American Type Culture Collection (ATCC, USA).

### 2.2 Preparation and Characterization of Polyblend Solutions

To be used chitosan (Ch) for polyblend was prepared of 1% (w/w) in 90 wt% acetic acid solution, and it stirred at 30 °C for 24 h. The 40 wt% PMSQ + 2 wt% BHA + 1 wt% Ch polyblend solutions, including weight-by-weight basis hBN as 0.1 (PCBB1), 0.2 (PCBB2), and 0.3 wt% (PCBB3), dissolved in DMC underwent vigorous stirring within a 24-h span at 50 °C. Finally, a colloidal solution was obtained, and it was suitable for the single-nozzle electrospinning process. The viscosities of the polyblend solutions were determined

using a calibrated Brookfield DV-E Viscometer (Brookfield Instruments, MA, USA) at room temperature (23 °C). The values for density were measured using a standard 25-mL density bottle.

### 2.3 Production of PCBB Hollow Microparticles

Production of PCBB hollow microparticles was performed by using the single-nozzle electrospinning method. Figure 2 shows a schematic of the experimental setup for single-nozzle electrospinning method. The selected electrospinning device (NS24, Istanbul, Turkey) consists of a grounded high-voltage power supply that generates positive DC applied voltages up to 60 kV (Fig. 2a). The flow of solutions through the nozzle with silicone tube was controlled by a one high-precision syringe pump (Fig. 2b; World Precision Instruments, Florida, USA). The diameters of the stainless steel nozzle were 3000  $\mu\text{m}$  for outer and 850  $\mu\text{m}$  for inner orifice (Fig. 2c). Sterile syringe (Set Medical Industry and Trade Inc., Istanbul, Turkey) was loaded into the syringe pump containing the polyblend solutions by 10-mL volume capacity. Applied voltage is an essential factor for the electrospinning process [15]. Therefore, when the applied voltage was higher than the threshold voltage, Taylor Cone will occur and electrospinning process can be started [52]. In this study, the applied voltage gradually increased until observing the

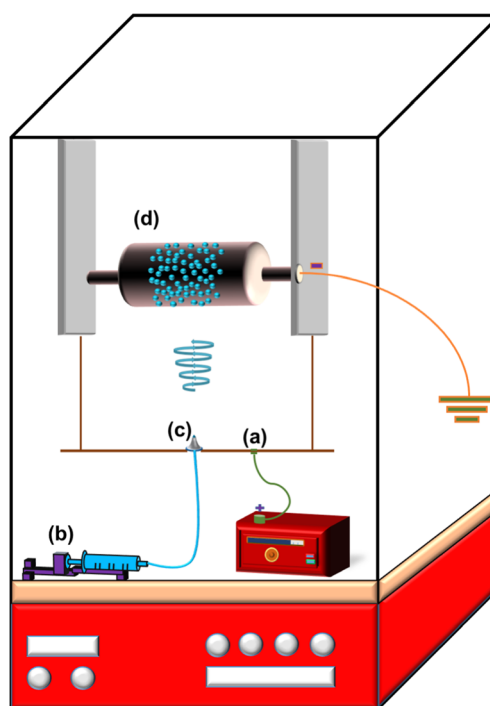


**Fig. 2** Single-nozzle electrospinning experimental setup working and non-working situations. **a** High-voltage power supply. **b** High-precision syringe pump. **c** Stainless steel nozzle. **d** Static continual collector

Taylor Cone before the experiments. On the other hand, other important parameters, such as flow rate and working distance, were also selected after different experiments on polymer solutions. Voltage value at which the Taylor cone was observed was taken as the experimental voltage value on 38.1 kV and the pump rate was fixed at 3.00 mL/h by the syringe pump. The working distance between the nozzle tip and the aluminum foil covered continual collector (Fig. 2d) was set to 19.5 cm for three experiments. For each processing, experiment and ambient conditions were carried out under the 23 °C temperature and 67.2% humidity. All the single-nozzle electrospinning parameters were determined and fixed same, for all the polyblend solutions to obtain a better observation for the thermal and mechanical properties of hBN. The PCBB1, PCBB2, and PCBB3 polyblend solutions were electrospun for 5 h, and then, obtained fiber and hollow microparticle samples were left under 50 °C in a laboratory oven for 24 h to remove the solvent, DMC. All experiments were repeated three times.

#### 2.4 Amoxicillin Loading to PCBB Hollow Microparticles

Of the amoxicillin, 40 mg was added to 10 mL PCBB3 polyblend solution. And final solution was stirred for 1 h at ambient temperature (23 °C). Ten-milliliter polyblend solution was loaded to electrospinning machine; the 3 mL solution was stayed at silicone tube and the rest of the polyblend solution (7 mL) were electrospun for 140 min. Working distance between the nozzle tip and the static continual collector was set to 19.5 cm; 42.2 kV was optimized for producing AMX loaded microparticles, since Taylor Cone occurring voltage value was on that rate and pump rate was fixed at 3.00 mL/h by syringe pump. After the single-nozzle electrospinning process, total weight of the obtained sample was 7 g.

#### 2.5 Dimensional Characterization of Hollow Microparticles With Scanning Electron Microscope and Optical Microscope

The morphology of the samples was characterized using a scanning electron microscope (SEM) (Carl Zeiss, OR, USA) and optical microscopy (The Olympus® Color View Microscope, USA). The samples for SEM were sputter coated with gold for 60 s with accelerating voltage of 3 kV (SC7620 Mini Sputter Coater, Quorum, UK).

#### 2.6 Determination of Hollow Microparticle Sizes

The size distributions of the hollow microparticle samples with and without AMX were measured using Litesizer™ 500 (Anton Paar GmbH, Graz, Austria). All samples were

prepared with 0.02-g hollow microparticles in 1 mL DCM concentration, and after the preparation, ultrasonic wave was applied to samples for 30 min. Each sample was analyzed in triplicate.

#### 2.7 Fourier Transform Infrared Spectroscopy

The functional groups and microparticle structure of samples were identified using IR Prestige 21 FTIR spectrophotometer (Shimadzu Corporation, Japan). The spectrum was recorded between 4000 and 650  $\text{cm}^{-1}$  with a resolution of 1  $\text{cm}^{-1}$  for each run at the ambient temperature (24 °C), and a number of the average scan was 100.

#### 2.8 X-Ray Diffraction Analysis

The X-ray diffraction analysis (XRD) patterns of pure PMSQ, pure BHA, pure Ch, pure hBN, and all PCBB samples were recorded on a PANalytical X'pert pro diffractometer (Atomika, Netherlands). The diffractometer involved monochromatic Cu-K $\alpha$  radiation ( $\lambda = 1.54056 \text{ \AA}$ ), a voltage of 45 kV, and current of 40 mA. The scanning rate was 3°/min and the scanning scope of  $2\theta$  was from 2° to 45° at room temperature (25 °C).

#### 2.9 In Vitro AMX Release at pH 7.4 From Hollow Microparticles

The release kinetics of model drug (AMX) from hollow microparticles was determined by recording the absorbance of AMX at 229 nm using a UV spectrophotometer (S-3100, Scinco, Korea). The hollow microparticles (60 mg), which are including 0.05627 mg AMX, were dispersed into 5 mL PBS (pH = 7.4) and samples were stirred to ensure constant incubation temperature (37 °C  $\pm$  0.2). To define the release of AMX from produced hollow microparticles, samples were centrifuged at 4000 rpm for 1800 s, the supernatant was removed, and accumulated release of AMX was evaluated using the calibration graph of a standard AMX, based on the absorbance peak area at a wavelength of 229 nm. The experiment was done three times. At the pre-determined time points up to 10 h, 3 mL of the solution of release medium was taken out from each vial and an equal volume of fresh PBS was replenished.

#### 2.10 Determination of Drug Loading Capacity/Encapsulation Efficiency/Yield of the Hollow Microparticles

The AMX content in hollow microparticle samples and the drug encapsulation efficiency (EE; %) were measured after extraction of a drug from the hollow microparticles. The drug



loading, encapsulation efficiency, and the yield of the process were determined with following equations [53]:

#### Drug Loading

$$= \frac{\text{Weight of AMX in Hollow Microparticles}}{\text{Total Weight of Microparticles}} \times 100 \quad (1)$$

#### Encapsulation Efficiency

$$= \frac{\text{Weight of AMX in Hollow Microparticles}}{\text{Weight of AMX Used}} \times 100 \quad (2)$$

$$\text{Yield} = \frac{\text{Weight of Hollow Microparticles}}{\text{Total Weight of Material}} \times 100 \quad (3)$$

### 2.11 In Vitro Antibacterial Activity Assay

*S. aureus* bacteria was used to determine the antibacterial activity of the all PCBB samples with and without AMX. For the analysis, the frozen *S. aureus* (ATCC 25923) was activated in brain heart infusion (BHI; Merck) agar at 37 °C for 24 h. After that, the bacterial concentration was adjusted to 0.5 McFarland standard and 0.1 mL bacteria were spread on MHA medium (Mueller-Hinton agar). Before the experiments, samples were sterilized with UV lights for 15 min. The samples (exactly 10 mg each one) were placed on the agar plate. After incubation at 37 °C for 24 h, the inhibition zones were measured.

### 2.12 Cell Culture and Biocompatibility Evaluation

U2OS, human bone osteosarcoma cell line, were cultured in DMEM supplemented with 10% FBS, 1% penicillin-streptomycin, and 1% L-glutamine. Of the cells,  $5 \times 10^4$  were seeded on 12-well culture plate in 1 mL medium and cells were incubated at 37 °C in a 5% CO<sub>2</sub> humidified incubator. Cells treated without or with 0.1 mg of PCBB3 and PCBB3 + AMX were evaluated for metabolic activity by using MTT colorimetric assay. MTT assay relies on the cellular oxidoreductase enzyme activity reflecting the presence of mitochondrial functionality in viable cells. These enzymes are capable of reducing the tetrazolium dye 3-(4,5-dimethylthiazol-2-yl)-2,5-diphenyltetrazolium bromide (MTT) to its insoluble purple formazan that can be evaluated by spectrophotometric analysis.

At 24 and 48 h post-treatment, MTT reagent was directly added to each well, and after incubation for additional 4 h at 37 °C, formazan was dissolved in dimethyl sulfoxide (DMSO) and then the absorbance was measured at 570/655 nm using an iMax Microplate Reader (Roche). Non-treated cells were used as a control and handled in the same way as their treated counterparts. In a parallel experiment, cultured cells were stained by addition of 1 µg/µL Hoechst

33342 and MitoTracker Red and further incubated for 30 min. After washing with PBS, nuclear morphology and mitochondria in live cells were visualized using confocal microscopy analysis (Carl-Zeiss LSM 710, Germany). Statistical analyses were performed using Student's two-tailed *t* test. Data were represented as means of ±SD of three independent experiments. Values with *p* < 0.05 were considered as significant.

## 3 Results and Discussion

It would be expected that both viscosity and density parameters for polyblend solution would be considered as important parameters to change of the fiber diameter and forming of fibers to microparticle transition in electrospinning [54]. Generally, by increasing the viscosity of the solution, the fibers occur with no bead formation [55]. However, in this study, increasing polyblend solution concentration with changing the hBN concentration as 0.1, 0.2, and 0.3 wt%, the viscosity of the solutions increases from  $16.89 \pm 0.07$  to  $29.42 \pm 0.05$  mPa s, fiber structure was started to making hollow microparticles (Fig. 3). Otherwise, density values for PCBB1, PCBB2, and PCBB3 polyblend solutions were measured as  $1.26 \pm 0.007$ ,  $1.27 \pm 0.009$ , and  $1.28 \pm 0.007$  g/mL, respectively, and for PCBB3 + AMX polyblend solution was  $1.3 \pm 0.007$  g/mL.

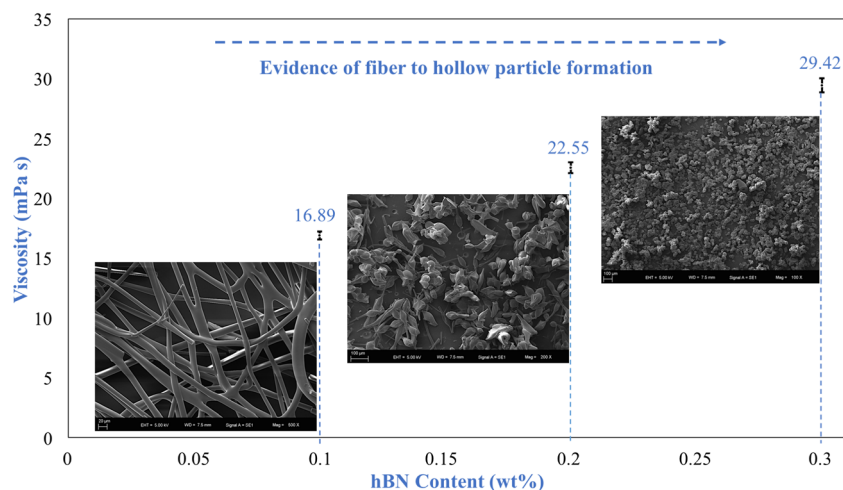
Chang et al. [56] has demonstrated production of hollow polymeric microspheres from PMSQ polymer by using a pair of nested concentric needles in electrospinning. Accordingly, they have never produced hollow solid microparticles with electrospinning below 63 wt% of PMSQ; in this study, hollow microparticles from 40 wt% PMSQ + 1 wt% Ch + 2 wt% BHA + 0.3 wt% hBN polyblend solution has been produced with single-nozzle electrospinning method.

Husain et al. [57] observed a parabolic rise in viscosity with using a different concentration of PLGA in acetone (2 to 25 wt%) resulting fiber formation with 25 wt% by electrospinning method. They described that higher viscosity causes fiber fracture because of ultimately the visco-elastic stresses are strong enough to prevent fiber fracture. In this study, higher viscosity caused prevention of particle formation. However, the polymer concentration is just one factor for fiber to particle formation. Changing the polymer can affect fiber formation by affecting the polymer-solvent interaction as observed by Koski et al. [58].

Remote image of the PCBB3 + AMX sample right after the single-nozzle electrospinning process can be seen in Fig. 4a. Figure 4b shows the close-up image of the sample, which seems like cotton surface, after left at under 50 °C in a laboratory oven, and Fig. 4c shows final product in a falcon tube.

Fiber to hollow microparticle formation of PCBB1, PCBB2, and PCBB3 are approved and shown in Fig. 5, with comparative optical microscopy and SEM images. As can be

**Fig. 3** Graphic of hollow microparticle formation with different viscosity values



seen on the images, while hBN concentration increases, fibers started to change their formation to hollow microparticles.

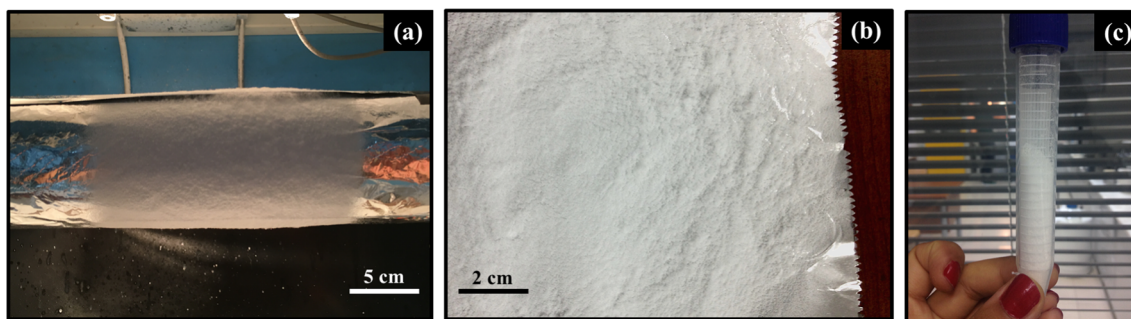
The mean diameter of the hollow microparticle samples was accounted for  $50 \pm 10 \mu\text{m}$  for PCBB3 sample (Fig. 6a) and  $90 \pm 10 \mu\text{m}$  for PCBB3 + AMX sample (Fig. 6b). Also, one selected particle of PCBB3 + AMX sample was imaged with SEM and that particle sample had a smooth surface (Fig. 6c),  $\sim 88\text{-}\mu\text{m}$  diameter size,  $\sim 53\text{-}\mu\text{m}$  passage hole with  $\sim 1\text{-}\mu\text{m}$  wall thickness (Fig. 6d).

Figure 7a shows Fourier transformation infrared spectroscopy (FTIR) spectra for a series of pure PMSQ, pure BHA, pure hBN, pure Ch, PCBB1, PCBB2, and PCBB3 to confirm the chemical composition of samples. Typical absorption peaks for PMSQ-related stretching modes were notable for of PCBB polyblend samples at around 2900, 1275, 1004, and  $760 \text{ cm}^{-1}$ . These can be due to the presence of characteristic C–H vibrations, Si–CH<sub>3</sub> symmetric deformation, Si–O–Si asymmetric stretch, and the Si–C stretch of PMSQ, respectively [59]. Although the PMSQ ratio is too much besides of other polymers in polyblend solutions, there was no big difference observed in FTIR spectra.

Figure 7b shows the characteristic peaks of PCBB3 hollow microparticle samples loaded with AMX and pure AMX. The peaks at 1685, 1773, and 2969 and peaks

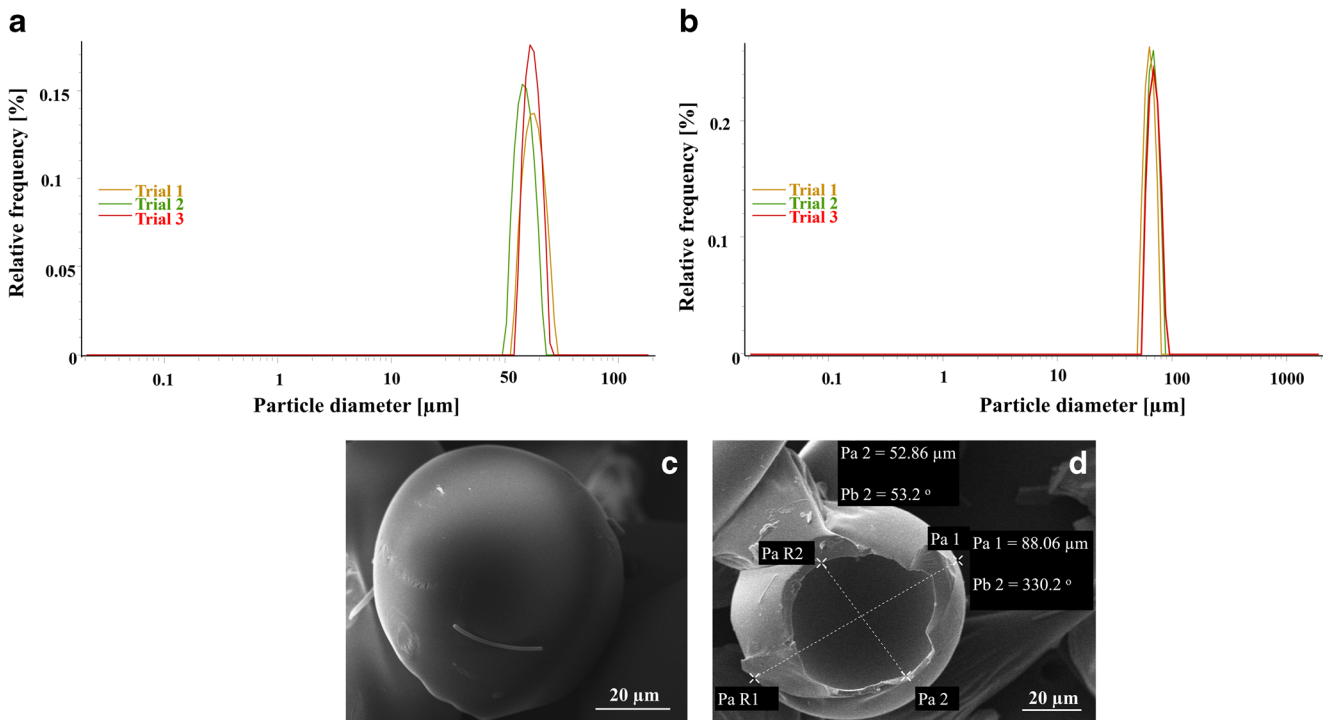
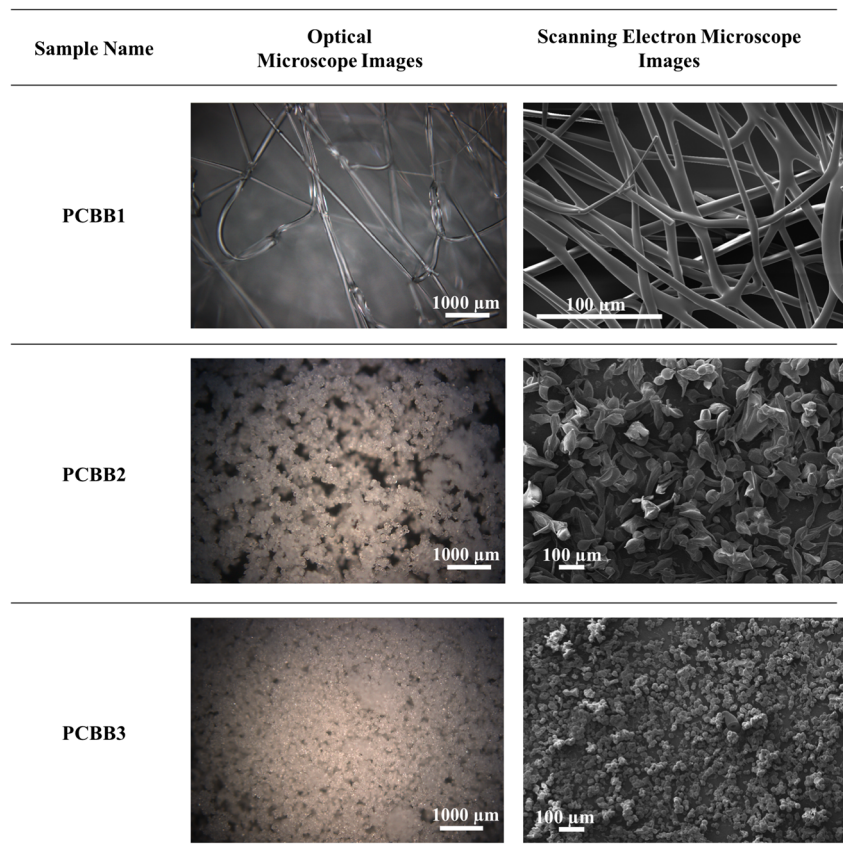
around  $3450 \text{ cm}^{-1}$  are attributed to AMX in hollow microparticle samples loaded with AMX [60]. When the drug and the polymer had chemically interacted with the functional groups, it has been expected that the FTIR spectra show band shifts and broadening, compared with the spectra of the pure drug and polymer [61]. Therefore, the results committed that there were no chemical interactions between AMX and produced hollow microparticles. Moreover, the spectra suggest that AMX is not decomposed while loading to the hollow microparticles using single-nozzle electrospinning method.

Figure 7c shows the comparable XRD patterns of pure BHA, pure hBN, and PCBB3 + AMX samples. The diffraction peaks for the existence of PMSQ were observable in PCBB3 + AMX sample at  $2\theta = 10.3$  and  $22.3$  [62]. hBN diffraction peaks were also detected at  $2\theta = 26, 41.7,$  and  $55.1$  in the sample [63]. In addition, some hardly visible diffraction peaks were observable for PCBB3 sample at  $2\theta = 31.7, 32.2,$  and  $40$ , which indicates the presence of BHA (JCPDS card number 98–005–2689). Because of the high percentage of PMSQ polymer, BHA can be dominated by PMSQ at XRD analysis, as previous work; Kim et al. fabricated polycaprolactone/hydroxyapatite (PCL/HA) scaffolds with



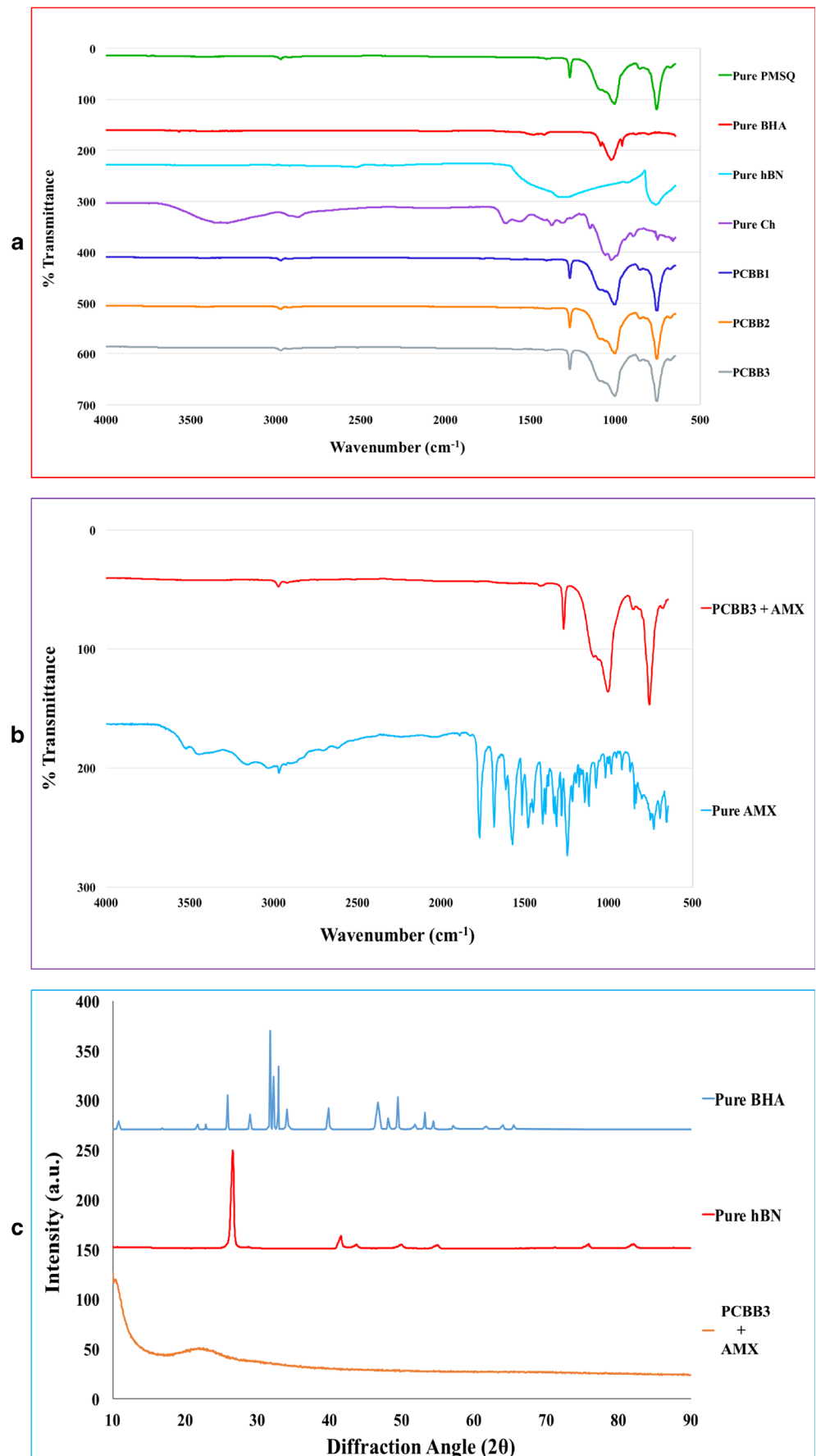
**Fig. 4** Macroscopic view of the electrospun PCBB3 + AMX sample. **a** Remote look. **b** Closer look. **c** Final product in a falcon tube

**Fig. 5** Comparative optical and SEM images of PCBB1, PCBB2, and PCBB3 samples



**Fig. 6** Particle diameters for the PCBB3 hollow microparticle sample (a) and PCBB3 + AMX microparticle sample (b). Micrographs of a selected hollow particle surface (c) with internal structure and diameters of passage hole of the hollow microparticle (d)

**Fig. 7** FTIR spectra for pure polymers (PMSQ, BHA, hBN, Ch), electrospun PCBB1, PCBB2, and PCBB3 polyblends (a). PCBB3 hollow microparticle samples loaded with AMX and pure AMX (b). X-ray diffraction patterns of pure BHA, hBN, and PCBB3 + AMX samples (c)

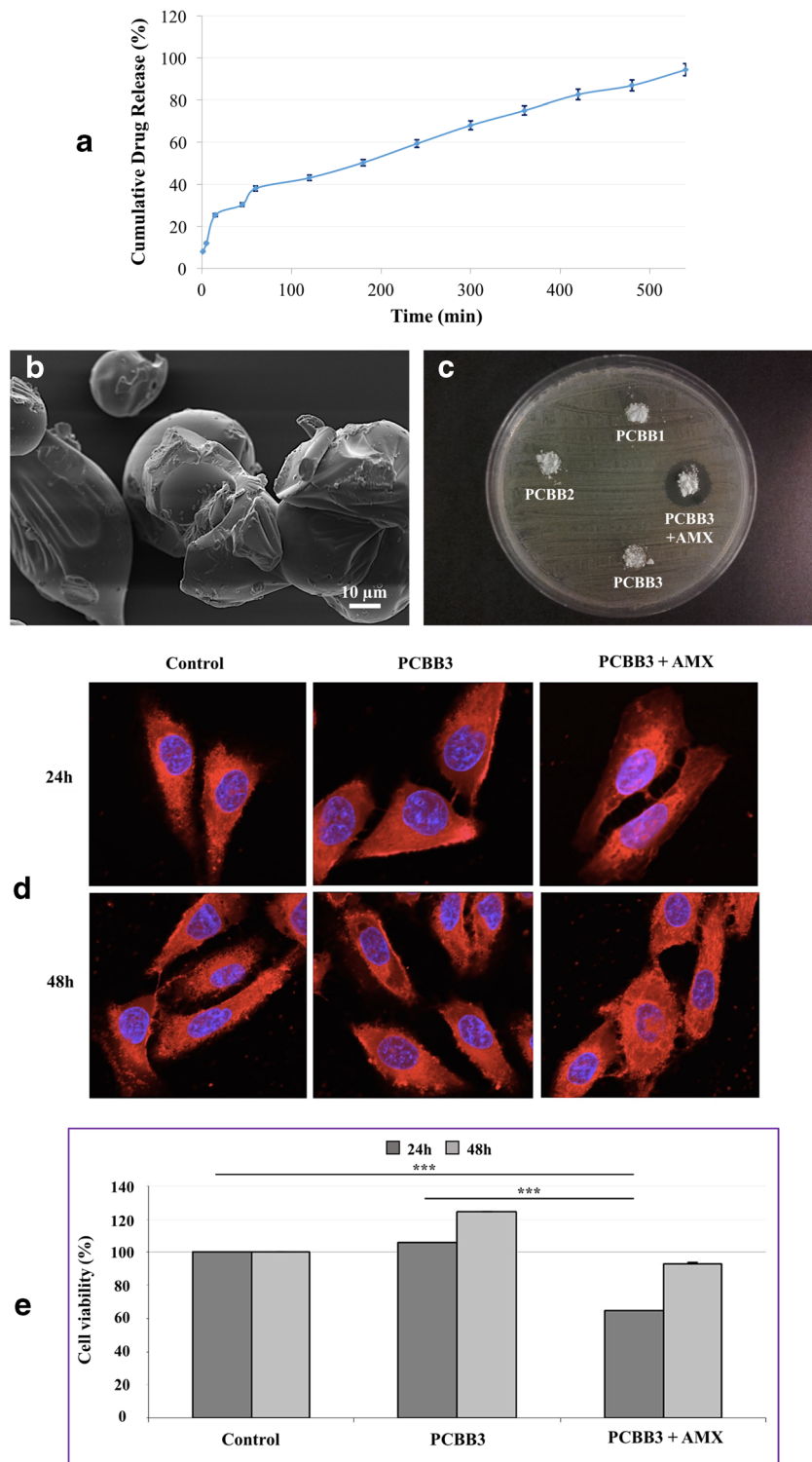




very low intensity diffraction peaks for existence HA in the composite, even if they have higher-percentage HA in composite than present work [64]. Hereby, alteration in the percentage of hBN has no obvious effect on the structure of PCB blend, and also, the blending of PMSQ, BHA, Ch, and hBN should not be the molecular-level blending.

AMX loaded hollow microparticles with an  $87 \pm 0.7\%$  encapsulation efficiency,  $52 \pm 1.9\%$  drug loading, and a  $68 \pm 1.1\%$  yield, indicating high encapsulation efficiency, good drug loading, and a high yield. The AMX loading value seemed well than the other works, AMX loading, for instance, the one worked by Farazuddin et al. with the

**Fig. 8** UV spectra for 229 nm of cumulative AMX release from hollow microparticles for 540 min (a) and SEM images of hollow microparticle structure after releasing their AMX (b). c Growth inhibition of bacterial (*S. aureus*) growth as a function of the AMX concentration after 24-h incubation of PCBB1, PCBB2, PCBB3, and PCBB3 + AMX samples. d Confocal microscopy images of U2OS cells after being cultured with PCBB3 and PCBB3 + AMX samples for 24 and 48 h. The viability of the PCBB3 and PCBB3 + AMX samples were 109 and 65% at the end of 24 h, respectively, and respective viabilities changed to 124 and 93% after 48 h (\*\*\* $P \leq 0.001$ )



value of  $42.0 \pm 5\%$  for PLGA microspheres via water-in-oil-in-water (W/O/W) emulsion method [65].

UV spectroscopic analysis indicated the presence of AMX in the hollow microparticles. To examine the release kinetics of AMX-loaded hollow microparticles, in vitro release of AMX loaded in hollow microparticles was observed in PBS at physiological temperature ( $37\text{ }^{\circ}\text{C}$ ) and pH (7.4) for 540 min. Figure 8a shows the release profiles demonstrating much AMX release rates with  $28 \pm 0.56$ ,  $50 \pm 1$ , and  $75 \pm 1.5\%$  being released by 60, 180, and 360 min, respectively, for both compositions and  $94 \pm 1.8\%$  release attained at 540 min. The AMX-loaded hollow microparticles were collected of the PBS medium after completing drug release studies, and samples were analyzed using SEM to clearly observe the structure after the drug had been released from them. Figure 8b shows the deformation of AMX-loaded hollow microparticle sample structure after releasing their AMX, and those microparticles were shown with some fractured shape and some preservation of structure after losing of their dry weight. For the antimicrobial activity of the PCBB1, PCBB2, PCBB3, and PCBB3 + AMX, concentrations were determined to measure of inhibition zone. As can be seen in Fig. 8c, PCBB1 and PCBB2 were not effective on bacterial growth, and PCBB3 was slightly effective on bacterial growth. However, PCBB3 + AMX sample inhibits the growth of the microorganism, and this result was promising for osteomyelitis disease treatment.

To assess biocompatibility of PCBB3 and its combination with AMX, U2OS cancer cells were cultured for 24 and 48 h in the absence or presence of 0.1 mg of PCBB3 and PCBB3 + AMX.

Compared to non-treated control cells, PCBB3 treatments did not have any detrimental effect at 24 h (Fig. 8d). However, as can be seen in Fig. 8e, the number of alive cells increased up to 124% after 48 h, indicating that the cells have active metabolism and can proliferate normally with PCBB3 treatment. On the other hand, encapsulation of PCBB3 with AMX significantly decreased U2OS cell viability until 65% at 24 h as compared to control. In other works, enhancement of cell viability of osteoblast with boron nitride nanotubes has been shown [66, 67]. However, there is no research with hBN and antibiotic combination for the biomedical application. Moreover, exposure of the cells for 48 h promoted the viability up to the 93%, indicating that cells are able to recover their metabolic activity and initiate their proliferation after 48 h of PCBB3 + AMX treatment.

As a consequence, PCBB3 and its encapsulation with AMX can be used as a promising drug model; yet, time of treatment should be seriously considered for better functional outcome in the case of therapeutic applications, as their effects are variable according to the lengths of treatment.

## 4 Conclusions

In the present study, AMX-loaded PCBB3 hollow microparticles were prepared by single-nozzle electrospinning method using different hBN concentrations (0.1, 0.2, and 0.3 wt%) to investigate their influence on particle formation, morphology, and drug release. It has been found that the hBN concentration affects the fiber to hollow microparticle transformation. Particles with different morphologies were obtained depending on the concentration of hBN, and the concentration of PCBB3 was selected to study thanks to its ability to produce most fine hollow microparticles. Hollow microparticles were produced with mean diameter of  $50 \pm 10\text{ }\mu\text{m}$ . The fine hollow internal microparticles of different size loaded with AMX as a model drug for investigating their drug release capability and the study have been successfully synthesized using the highly efficient (encapsulation efficiency  $87 \pm 0.7\%$ ). In conclusion, with the significantly reduced drug release profile, good cytocompatibility, and the remained antibacterial activity, the developed hollow microparticles should find potential application for drug delivery, antimicrobial effect, and bone repair for osteomyelitis disease treatment at the same time with AMX.

## Compliance with Ethical Standards

**Conflict of Interest** The authors declare that they have no conflict of interests.

## References

1. Zhu-Zhu, L., Li-Xiong, W., Lei, S., & Jian-Feng, C. (2004). Fabrication of porous hollow silica nanoparticles and their applications in drug release control. *Journal of Controlled Release*, *98*, 245–254.
2. Lou, X. W., Archer, L. A., & Yang, Z. (2008). Hollow micro/nanostructures: Synthesis and applications. *Advanced Materials*, *20*, 3987–4019.
3. Enayati, M., Ahmad, Z., Stride, E., & Edirisinghe, M. (2010). One-step electrohydrodynamic production of drug-loaded micro- and nanoparticles. *Journal of the Royal Society, Interface*, *7*, 667–675.
4. Bohr, A., Kristensen, J., Stride, E., Dyas, M., & Edirisinghe, M. (2011). Preparation of microspheres containing low solubility drug compound by electrohydrodynamic spraying. *International Journal of Pharmaceutics*, *412*, 59–67.
5. Fujiwara, M., Shiokawa, K., Tanaka, Y., & Nakahara, Y. (2004). Preparation and formation mechanism of silica microcapsules (hollow sphere) by water/oil/water interfacial reaction. *Chemistry of Materials*, *16*, 5420–5426.
6. Im, S. H., Jeong, U., & Xia, Y. (2005). Polymer hollow particles with controllable holes in their surfaces. *Nature Materials*, *4*, 671–675.
7. Roy, P., Bertrand, G., & Coddet, C. (2005). Spray drying and sintering of zirconia based hollow powders. *Powder Technology*, *157*, 20–26.
8. Nagamine, S., Sugioka, A., & Konishi, Y. (2007). Preparation of TiO<sub>2</sub> hollow microparticles by spraying water droplets into an

- organic solution of titanium tetraisopropoxide. *Materials Letters*, 61, 444–447.
9. Zhang, L., D'Acunzi, M., Kappl, M., Auernhammer, G. K., Vollmer, D., van Kats, C. M., & van Blaaderen, A. (2009). Hollow silica spheres: Synthesis and mechanical properties. *Langmuir*, 25, 2711–2717.
  10. Lin, Y. S., Wu, S. H., Tseng, C. T., Hung, Y., Chang, C., & Mou, C. Y. (2009). Synthesis of hollow silica nanospheres with a microemulsion as the template. *Chemical Communications*, 24, 3542–3544.
  11. Mathiowitz, E., Jacob, J. S., Jong, Y. S., Carino, G. P., Chickering, D. E., Chaturvedi, P., Santos, C. A., Vijayaraghavan, K., Montgomery, S., Bassett, M., & Morrell, C. (1997). Biologically erodable microspheres as potential oral drug delivery systems. *Nature*, 386, 410–414.
  12. Marinakos, S. M., Novak, J. P., Brousseau III, L. C., House, A. B., Edeki, E. M., Feldhaus, J. C., & Feldheim, D. L. (1999). Gold particles as templates for the synthesis of hollow polymer capsules. Control of capsule dimensions and guest encapsulation. *Journal of the American Chemical Society*, 121, 8518–8522.
  13. Kim, S. W., Kim, M., Lee, W. Y., & Hyeon, T. (2002). Fabrication of hollow palladium spheres and their successful application to the recyclable heterogeneous catalyst for Suzuki coupling reactions. *Journal of the American Chemical Society*, 124, 7642–7643.
  14. Yow, H. N., Wu, X., Routh, A. F., & Guy, R. H. (2009). Dye diffusion from microcapsules with different shell thickness into mammalian skin. *European Journal of Pharmaceutics and Biopharmaceutics*, 72, 62–68.
  15. Yu, M., Dong, R.-H., Yan, X., Yu, G.-F., You, M.-H., Ning, X., & Long, Y.-Z. (2017). Recent advances in needleless electrospinning of ultrathin fibers: From academia to industrial production. *Macromolecular Materials and Engineering*, 302, 1–19.
  16. Pillay, V., Dott, C., Choonara, Y. E., Tyagi, C., Tomar, L., Kumar, P., du Toit, L. C., & Ndesendo, V. M. K. (2013). A review of the effect of processing variables on the fabrication of electrospun Nanofibers for drug delivery applications. *Journal of Nanomaterials*, 2013, 1–22.
  17. Vilara, G., Tulla-Puche, J., & Albericio, F. (2012). Polymers and drug delivery systems. *Current Drug Delivery*, 9, 1–28.
  18. Zawaneh, P. N., Doody, A. M., Zelikin, A. N., & Putnam, D. (2006). Diblock copolymers based on dihydroxyacetone and ethylene glycol: Synthesis, characterization, and nanoparticle formulation. *Biomacromolecules*, 7, 3245–3325.
  19. Xiang, H., Zhang, L., Wang, Z., Yu, X., Long, Y., Zhang, X., & Xu, J. (2011). Multifunctional polymethylsilsesquioxane (PMSQ) surfaces prepared by electrospinning at the sol–gel transition: Superhydrophobicity, excellent solvent resistance, thermal stability and enhanced sound absorption property. *Journal of Colloid and Interface Science*, 359, 296–303.
  20. Cross, S. E., Innes, B., Roberts, M. S., Tsuzuki, T., Robertson, T. A., & McCormick, P. (2007). Human skin penetration of sunscreen nanoparticles: In-vitro assessment of a novel micronized zinc oxide formulation. *Skin Pharmacology and Physiology*, 20, 148–154.
  21. Cheng, C. J., Chu, L. Y., & Xie, R. (2006). Preparation of highly monodisperse W/O emulsions with hydrophobically modified SPG membranes. *Journal of Colloid and Interface Science*, 300, 375–382.
  22. Chen, J.-F., Ding, H.-M., Wang, J.-X., & Shao, L. (2004). Preparation and characterization of porous hollow silica nanoparticles for drug delivery application. *Biomaterials*, 25, 723–727.
  23. Geng, H., Zhao, Y., Liu, J., Cui, Y., Wang, Y., Zhao, Q., & Wang, S. (2016). Hollow mesoporous silica as a high drug loading carrier for regulation insoluble drug release. *International Journal of Pharmaceutics*, 510, 184–194.
  24. Zhao, Q., Geng, H., Wang, Y., Gao, Y., Huang, J., Wang, Y., Zhang, J., & Wang, S. (2014). Hyaluronic acid oligosaccharide modified redoxresponsive mesoporous silica nanoparticles for targeted drug delivery. *ACS Applied Materials & Interfaces*, 6, 20290–20299.
  25. Echeverria, C., Soares, P., Robalo, A., Pereira, L., Novo, C. M. M., Ferreira, I., & Borges, J. P. (2015). One-pot synthesis of dual-stimuli responsive hybridPNIPAAm-chitosan microgels. *Materials and Design*, 86, 745–751.
  26. Rinaudo, M. (2006). Chitin and chitosan: Properties and applications. *Progress in Polymer Science*, 31, 603–632.
  27. Depan, D., & Misra, R. D. K. (2012). Hybrid nanostructured drug carrier with tunable and controlled drug release. *Materials Science and Engineering: C*, 32, 1704–1709.
  28. Misra, R. D. K. (2012). Core–shell magnetic nanoparticle carrier for targeted drug delivery: Challenges and design. *Materials and Technologies*, 25, 118–126.
  29. Torrado, S., Prada, P., Torre, P. M., & Torrado, S. (2004). Chitosan-poly(acrylic) acid polyionic complex: In vivo study to demonstrate prolonged gastric retention. *Biomaterials*, 25, 917–923.
  30. Venugopal, J., Prabhakaran, M. P., Zhang, Y., Low, S., Choon, A. T., & Ramakrishna, S. (2010). Biomimetic hydroxyapatite-containing composite nanofibrous substrates for bone tissue engineering. *Philosophical Transactions of the Royal Society A*, 368, 2065–2208.
  31. Hwang, H. J., Barakat, N. A. M., Kanjwal, M. A., Sheikh, F. A., & Kim, Y. H. (1992). Boron nitride nanofibers by the electrospinning technique. *Macromolecular Research*, 18, 551–557.
  32. Kawanabe, K., Okada, Y., Matsusue, Y., Iida, H., & Nakamura, T. (1998). Treatment of osteomyelitis with antibiotic soaked porous glass ceramic. *Journal of Bone and Joint Surgery*, 80-B, 30–527.
  33. Chang, Y. L., Stanford, C. M., & Keller, J. C. (2000). Calcium and phosphate supplementation promotes bone cell mineralization: Implications for hydroxyapatite (HA)-enhanced bone formation. *Journal of Biomedical Materials Research*, 52, 8–270.
  34. Goto, T., Kojima, T., Iijima, T., Yokokura, S., Kawano, H., Yamamoto, A., & Matsuda, K. (2001). Resorption of synthetic porous hydroxyapatite and replacement by newly formed bone. *Journal of Orthopaedic Science*, 6, 7–444.
  35. Catanese, J., Featherstone, J. D. B., & Keavery, T. M. (1999). Characterization of the mechanical and ultrastructural properties of heat treated cortical bone for use as a bone substitute. *Journal of Biomedical Materials Research*, 45, 36–327.
  36. Hwang, H. J., Barakat, N. A. M., Kanjwal, M. A., Sheikh, F. A., & Kim, Y. H. (2010). Boron nitride nanofibers by the electrospinning technique. *Macromolecular Research*, 18, 551–557.
  37. Kumar, V., Abbas, A., & Fausto, N. (2007). *Robbins basic pathology* (8th ed.). Philadelphia: Elsevier Health.
  38. Romano, C. L., Romanò, D., Logoluso, N., & Drago, L. (2011). Bone and joint infections in adults: A comprehensive classification proposal. *European Orthopaedics and Traumatology*, 1, 207–217.
  39. Lew, D. P., & Waldvogel, F. A. (2004). Osteomyelitis. *Lancet*, 364, 79–369.
  40. Mader, J. T., Mohan, D., & Calhoun, J. (1997). A practical guide to the diagnosis and management of bone and joint infections. *Drugs*, 54, 253–264.
  41. Cassat, J. E., Hammer, N. D., Campbell, J. P., Benson, M. A., Perrien, D. S., Mrak, L. N., Smeltzer, M. S., Torres, V. J., & Skaar, E. P. (2013). *Cell Host & Microbe*, 13, 759–772.
  42. Horst, S. A., Hoerr, V., Beineke, A., Kreis, C., Tuchscher, L., Kalinka, J., Lehne, S., Schleicher, I., Köhler, G., Fuchs, T., Raschke, M. J., Rohde, M., Peters, G., Faber, C., Löffler, B., & Medina, E. (2012). A novel mouse model of Staphylococcus aureus chronic osteomyelitis that closely mimics the human infection. *The American Journal of Pathology*, 181, 1206–1214.
  43. Gerber, J. S., Coffin, S. E., Smathers, S. A., & Zaoutis, T. E. (2009). Trends in the incidence of methicillin-resistant Staphylococcus aureus infection in children's hospitals in the United States. *Clinical Infectious Diseases*, 49, 65–71.

44. Weichert, S., Sharland, M., Clarke, N. M., & Faust, S. N. (2008). Acute haematogenous osteomyelitis in children: Is there any evidence for how long we should treat? *Current Opinion in Infectious Diseases*, 21, 258–262.
45. Rao, N., Ziran, B. H., & Lipsky, B. A. (2011). Treating osteomyelitis: Antibiotics and surgery. *Plastic and Reconstructive Surgery*, 127, 177S–187S.
46. Brady, R. A., Leid, J. G., Costerton, J. W., & Shirliff, M. E. (2006). Osteomyelitis: Clinical overview and mechanisms of infection persistence. *Clinical Microbiology Newsletter*, 28, 65–72.
47. Gunduz, O., Ahmad, Z., Stride, E., & Edirisinghe, M. (2013). Continuous generation of ethyl cellulose drug delivery Nanocarriers from microbubbles. *Pharmaceutical Research*, 30, 225–237.
48. Cohen, R., & Grimprel, E. (2007). Pharmacokinetics and pharmacodynamics of antimicrobial therapy used in child osteoarticular infections. *Archives de Pédiatrie*, 14, 122–127.
49. Landersdorfer, C. B., Kinzig, M., Bulitta, J. B., Hennig, F. F., Holzgrabe, U., Sorgel, F., & Gusinde, J. (2009). Bone penetration of amoxicillin and Clavulanic acid evaluated by population pharmacokinetics and Monte Carlo simulation. *Antimicrobial Agents and Chemotherapy*, 53, 2569–2578.
50. Lipsky, B., Itani, K., & Norden, C. (2004). Treating foot infections in diabetic patients: A randomized, multicenter, open-label trial of linezolid versus ampicillin-sulbactam/amoxicillin-clavulanate. *Clinical Infectious Diseases*, 38, 17–24.
51. Gisby, J., Beale, A. S., Bryant, J. E., & Toseland, C. D. (1994). Staphylococcal osteomyelitis—A comparison of co-amoxiclav with clindamycin and flucloxacillin in an experimental rat model. *The Journal of Antimicrobial Chemotherapy*, 34, 755–764.
52. Li, Z., & Wang, C. (2013). *One-dimensional nanostructures. Effects of working parameters on electrospinning* (pp. 15–28). London: SpringerBriefs in Materials.
53. Luan, X., Skupin, M., Siepmann, J., & Bodmeier, R. (2006). Key parameters affecting the initial release (burst) and encapsulation efficiency of peptide-containing poly (lactide-co-glycolide) microparticles. *International Journal of Pharmaceutics*, 324, 168–175.
54. Soares, R. M. D., Patzer, V. L., Dersch, R., Wendorff, J., Silveira, N. P., & Pranke, P. (2011). A novel globular protein electrospun fiber mat with the addition of polysilsesquioxane. *International Journal of Biological Macromolecules*, 49, 480–486.
55. Fong, H., Chun, I., & Reneker, D. H. (1999). Beaded nanofibers formed during electrospinning. *Polymer*, 40, 4585–4592.
56. Chang, M. W., Stride, E., & Edirisinghe, M. (2010). Controlling the thickness of hollow polymeric microspheres prepared by electrohydrodynamic atomization. *Journal of the Royal Society, Interface*, 7, S451–S460.
57. Husain, O., Lau, W., Edirisinghe, M., & Parhizkar, M. (2016). Investigating the particle to transition threshold during electrohydrodynamic atomization of a polymer solution. *Materials Science and Engineering: C*, 65, 240–250.
58. Koski, A., Yim, K., & Shivkumar, S. (2004). Effect of molecular weight on fibrous PVA produced by electrospinning. *Materials Letters*, 58, 493–497.
59. Liang, T., Li, Y. L., Su, D., & Du, H. B. (2010). Silicon oxycarbide ceramics with reduced carbon by pyrolysis of polysiloxanes in water vapour. *Journal of the European Ceramic Society*, 30, 2677–2682.
60. Bebu, A., Szabó, L., Leopold, N., Berindean, C., & David, L. (2011). IR, Raman, SERS and DFT study of amoxicillin. *Journal of Molecular Structure*, 993, 52–56.
61. Silverstein, R. M., Bassler, G. C., & Morrill, T. C. (1991). *Spectrometric identification of organic compound*. New York: Wiley.
62. Wang, J., & Xin, Z. (2012). Synthesis and characterization of polymethylsilsesquioxane microspheres by the two-step sol-gel method. *E-Polymers*, 46, 1–10.
63. Kostoglou, N., Polychronopoulou, K., & Rebolz, C. (2015). Thermal and chemical stability of hexagonal boron nitride (h-BN) nanoplatelets. *Vacuum*, 112, 42–45.
64. Kim, J. Y., Lee, T. J., Cho, D. W., & Kim, B. S. (2010). Solid free-form fabrication-based PCL/HA scaffolds fabricated with a multi-head deposition system for bone tissue engineering. *Journal of Biomaterials Science, Polymer Edition*, 21, 951–962.
65. Farazuddin, M., Chauhan, A., Khan, R. M. M., & Owais, M. (2011). Amoxicillin-bearing microparticles: Potential in the treatment of listeria monocytogenes infection in Swiss albino mice. *Bioscience Reports*, 31, 265–272.
66. Lahiri, D., Rouzaud, F., Richard, T., Keshri, A. K., Bakshi, S. R., Kos, L., & Agarwal, A. (2010). Boron nitride nanotube reinforced polylactide–polycaprolactone copolymer composite: Mechanical properties and cytocompatibility with osteoblasts and macrophages in vitro. *Acta Biomaterialia*, 6, 3524–3533.
67. Lahiri, D., Singh, V., Benaduce, A. P., Seal, S., Kos, L., & Agarwal, A. (2011). Boron nitride nanotube reinforced hydroxyapatite composite: Mechanical and tribological performance and in-vitro biocompatibility to osteoblasts. *Journal of the Mechanical Behavior of Biomedical Materials*, 4, 44–56.